

pubs.acs.org/Macromolecules Article

Role of Grafting Density and Nitrile Functionalization on Gas Transport in Polymers with Side-Chain Porosity

Kayla R. Storme, Sharon Lin, You-Chi Mason Wu, Sherrie X. Qian, Timothy M. Swager,* and Zachary P. Smith*



Cite This: Macromolecules 2024, 57, 2458-2467



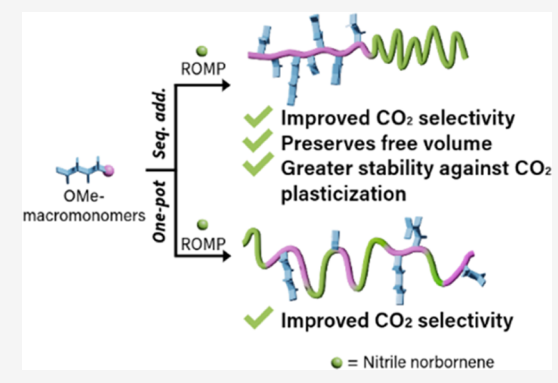
ACCESS I

III Metrics & More

Article Recommendations

s Supporting Information

ABSTRACT: This study details the enhancement of CO_2 selectivity in ring-opening metathesis polymerization (ROMP) polymers that contain nitrile moieties and micropore-generating ladder side chains. A material, CN-ROMP homopolymer, with nitriles in the ladder side chains was originally targeted and synthesized; however, its low molecular weight and backbone rigidity precluded film formation. As a result, an alternative method was pursued wherein copolymers were synthesized using norbornene (N) and nitrile norbornene (NN). Herein, we report an investigation of the structure—property relationships of backbone functionalization and grafting density on the CO_2 transport properties in these ROMP polymers. Nitrile-containing copolymers showed an increase in CO_2/CH_4 sorption selectivity and a concomitant increase in CO_2/CH_4 permselectivity when compared to the unfunctionalized (nitrile-free) analogues. The stability in CO_2 -rich environ-



ments is enhanced as grafting density of the rigid, pore-generating side chains increases and an apparent tunability of CO_2 plasticization pressure was observed as a function of norbornene content. Lower loadings of norbornene resulted in higher plasticization pressure points. Gas permeability in the ROMP copolymers was found to correlate most strongly with the concentration of the ladder macromonomers in the polymer chain.

INTRODUCTION

Heat-intensive separation technologies, such as distillation, consume roughly 50% of the energy in chemical and petrochemical separations in the U.S. and contribute extensively to greenhouse gas (GHG) emissions. Energyefficient alternatives will be crucial to meet the 80% emissions reduction target for 2050 set by the U.S. Department of Energy.² Compared to legacy separation processes, membranes are a promising option that have smaller footprints, do not require solvent regeneration, and do not rely on phase changes or moving parts to perform separations.^{3–5} However, to reduce capital and operating costs, membrane materials must be highly permeable and selective for the products of interest.^{4,6} In recent years, researchers have focused on efforts to develop high free-volume polymers often termed polymers of intrinsic microporosity (PIMs). The free volume in these systems is achieved by integrating three-dimensional rigid features that are fused into the polymer backbone to create structures that promote stochastic pore formation through inefficient chain packing,⁷ thereby enhancing gas permeability.⁸ Benzotriptycene-based PIMs,9 thermally rearranged (TR) polymers,10 and catalytic arene-norbornene annulation (CANAL) polymers¹¹ demonstrate remarkable improvements to gas separation performance. Despite exceptional advancements in permeability-selectivity property sets, there are still outstanding

questions related to material stability under relevant environments. $^{12-14}$ In 2018, we reported a class of bottlebrush polymers with rigid side chains via ring-opening metathesis polymerization (ROMP) 15 that showed high CO₂ permeability and an impressive resistance to CO₂-induced plasticization. In fact, at 35 °C, no CO₂ plasticization pressure was observed up to the maximum testing pressure of 51 bar. 16 In follow-up studies with CO₂/CH₄ mixture testing, we further demonstrated that the stability against CO₂-induced plasticization is modulated by the length of the pore-generating side chains in these ROMP systems. 17,18 Unfortunately, the ROMP polymers exhibit only moderate selectivity for CO₂ when compared to other state-of-the-art PIMs.

Promising approaches to increase the CO_2 selectivity in glassy polymers include incorporation of CO_2 -philic groups into the polymer structure. To this end, researchers have postsynthetically functionalized the PIM-1 architecture by converting native nitrile groups in the polymer backbone into

Received: November 15, 2023 Revised: February 7, 2024 Accepted: February 8, 2024 Published: March 1, 2024





Scheme 1. Synthesis of (a) CN-ROMP and (b) Norbornene (N)- and Nitrile Norbornene (NN)-Based Copolymers (a)

(b)
$$\frac{\text{Mes}^{-N} \cdot \text{Mes}}{\text{CI} \cdot \text{Ru} \cdot \text{Ph}}$$

$$\frac{\text{OMe}}{\text{OMe}} \cdot \frac{\text{OMe}}{\text{OMe}} \cdot \frac{\text{OMe}}{\text{CHCI}_3}$$

$$\frac{\text{OMe}}{\text{CHCI}_3} \cdot \frac{\text{OMe}}{\text{Res}^{-N} \cdot \text{NMes}}$$

$$\frac{\text{OMe}}{\text{CHCI}_3} \cdot \frac{\text{OMe}}{\text{Neo}} \cdot$$

amidoximes (PIM-AO), 19 thioamides (PIM-TA), 20 carboxylic acids (PIM-COOH), $^{21-23}$ and amines (PIM-NH₂). 24 Mizrahi Rodriguez et al. evaluated the structure—property relationships between different chemistries and identified CO₂ sorption affinity increases from carboxylic acid < nitrile < amine. 25 Since each functional group discussed previously can be made from a nitrile precursor, similar sorption advancements could be envisioned for the poly(ladder) ROMP family if nitriles could be incorporated into the polymer, which is the aim of this study.

Therefore, we installed nitrile moieties along the rigid side chains using graft-through polymerization methods to afford CN-ROMP (Scheme 1a) and we installed nitrile moieties in the backbone through copolymerization (Scheme 1b) with commercial nitrile norbornene (NN). CN-ROMP has a Brunauer-Emmett-Teller (BET) surface area of 791 m² g⁻¹ (Figure S1a and Table S1), which is higher than the previously studied OMe- and CF₃-ROMPs, ¹⁶ and thus a record for the ladder side-chain approach. However, we were unable to obtain flexible, free-standing films for further characterization. Consequently, our gas separation results focus on the copolymerization method to incorporate nitrile moieties. Poly(NN) was identified as an oxygen-selective membrane in 1988, but it displayed low permeability likely due to strong dipole-dipole interactions from the nitrile moieties and close packing of the polymer chains.²⁶ Kawakami et al. demonstrated that the permeability of poly(NN) could be enhanced by introducing bulky, rigid groups at the methylene α to the nitrile-bearing carbon of the norbornene monomer.²⁶ To the best of our knowledge, nitrile norbornene has not been examined in the context of CO₂/CH₄ separations. Considering the high CO₂ permeability and ease of synthesis of OMe-

ROMP, 16-18 it was a good candidate for copolymerization with NN to disrupt dense packing of poly(NN) chains. Copolymers with different amounts of NN content were synthesized, and simple norbornene (N) analogues were prepared to evaluate the effect of the nitriles. We first demonstrate the NN-based copolymer made with 50 wt % loading of NN displays higher CO2 sorption and CO2/CH4 sorption selectivity than the N-based analogue. We observed increases in CO₂/CH₄ selectivity in all NN-based copolymers compared to those in N-based copolymers, supporting the role of the nitrile on CO2-enhanced transport. Decreasing the loading of NN and N comonomers resulted in increased CO₂ permeability with a minimal change in CO₂/CH₄ selectivity. We also found that CO₂ plasticization pressures were tunable in N-based copolymers when varying loading of N, whereas the NN-based copolymers did not exhibit this behavior. To evaluate the impact of increasing grafting density on gas transport, we synthesized an NN-based block copolymer using 50 wt % NN loading and observed a reduction of CO₂/CH₄ selectivity relative to the statistical copolymer. This result reflects the similar increases in diffusivity of both CO2 and CH₄ with the availability of larger pores generated by neighboring rigid side chains.

EXPERIMENTAL SECTION

Materials. Dicyclopentadiene, sodium hydride (60% in mineral oil), 2-norbornene, and Grubbs second-generation catalyst were purchased from Millipore Sigma. Methyl iodide was purchased from TCI Chemicals; 5-norbornene-2-carbonitrile was purchased from TCI Chemicals and Combi-Blocks; magnesium sulfate and cesium carbonate were purchased from Macron Fine Chemicals; and acetonitrile (MeCN) was purchased from Alfa Aesar in a ChemSeal bottle. Anhydrous tetrahydrofuran (THF) and anhydrous dichloro-

methane (DCM) were obtained from an INERT PureSolv MDS solvent purification system and stored under argon over 4 Å molecular sieves. Chloroform was purchased from Millipore Sigma and sparged with argon for at least 30 min prior to use. 1,4-Anthraquinone was purchased from Combi-Blocks and purified with a silica plug using DCM as the eluent prior to use. HPLC-grade THF and HPLC-grade chloroform were purchased from J. T. Baker. All other solvents and reagents were purchased at ACS grade or higher and used as received.

Synthesis of Polymers. The following method was used to synthesize CN-ROMP: dried CN-ROMP macromonomers (220 mg, 0.2 mmol, 1 equiv) were added to an oven-dried vial with a stir bar under nitrogen atmosphere in a glovebox. The macromonomers were dissolved in 1.9 mL of anhydrous DCM. Schrock's catalyst (1.1 mg, 0.002 mmol, 0.01 equiv) was added to a vial in the glovebox and dissolved in 0.3 mL of anhydrous DCM. The catalyst solution was injected into the macromonomer solution and stirred overnight in the glovebox. The solution was quenched with 1 drop of benzaldehyde. CN-ROMP was purified using chloroform preparative GPC. Collected fractions were concentrated in vacuo and precipitated in methanol (100 mg yield).

NN-based statistical copolymers NN-3 and NN-13 were prepared using 27.5 and 50 wt % of NN, respectively. An example of the copolymerization procedure follows. A Schlenk flask was charged with the macromonomers (500.7 mg, 0.3 mmol) and sealed. The flask was evacuated and backfilled three times with argon. Solids were dissolved in 15 mL of sparged chloroform. 5-Norbornene-2-carbonitrile (0.5 mL, 4.2 mmol) was injected into the Schlenk flask, followed by three freeze-pump—thaw cycles. A solution of the Grubbs second-generation catalyst (2.547 mg, 0.003 mmol) in 2.5 mL of sparged chloroform was prepared and injected into the flask. The reaction mixture was stirred at room temperature overnight. The reaction was quenched with ethyl vinyl ether and stirred for an additional 30 min before diluting with DCM and precipitating in methanol. The resulting NN copolymer was dried under a vacuum overnight (824.3 mg yield).

N-based statistical copolymers N-3 and N-19 were prepared using 26.3 and 50 wt % of N, respectively. An example of the copolymerization procedure follows. A Schlenk flask was charged with the macromonomers (494.7 mg, 0.3 mmol) and 2-norbornene (494.7 mg, 5.2 mmol) under an argon atmosphere. The monomers were degassed and backfilled with argon three times before being dissolved in 15 mL of sparged chloroform. A solution of the Grubbs second-generation catalyst (2.687 mg, 0.003 mmol) in 2.5 mL of sparged chloroform was prepared and injected into the flask. The reaction was stirred at room temperature overnight. The reaction was quenched with ethyl vinyl ether and stirred for an additional 30 min before diluting with DCM and precipitating in methanol. The resulting N copolymer was dried under vacuum overnight (862.7 mg yield).

Block copolymer NNb-24 was synthesized using the following method: a Schlenk flask charged with the macromonomers (614.1 mg, 0.49 mmol, 1.0 equiv) was transferred into a glovebox under nitrogen atmosphere. The macromonomers were dissolved in 18 mL of dry THF before injecting a 2.8 mL THF solution containing Grubbs second-generation catalyst (4.160 mg, 0.0049 mmol, 0.01 equiv) into the flask. After ~15.5 h, consumption of macromonomers was observed via thin-layer chromatography (TLC) and 5-norbornene-2-carbonitrile (0.61 mL, 5.1 mmol, 10.41 equiv) was injected into the flask. The solution was removed from the glovebox and quenched with ethyl vinyl ether after 20 min. The quenched solution was stirred for an additional 30 min before diluting with DCM and precipitating in methanol. The NN block copolymer was dried under vacuum overnight (818.7 mg yield).

Polymer Film Preparation. Copolymer solutions containing 2 wt % polymer were prepared in chloroform and cast into flat-bottom PTFE Petri dishes. After 1–2 days of slow evaporation at room temperature in a fume hood, stable, free-standing, and defect-free films were formed. Each film was soaked in methanol for 24 h and then air-dried in a fume hood for 24 h before testing.

Chemical Characterization. The chemical structure was studied using ¹H and ¹³C nuclear magnetic resonance (NMR) spectroscopy in a 400 MHz two-channel Bruker Avance-III HD Nanobay spectrometer or a 600 MHz four-channel Bruker Avance Neo spectrometer. HMBC, HSQC, and COSY NMR were also used and collected on a 600 MHz four-channel Bruker Avance Neo spectrometer. Samples were prepared in deuterated chloroform and referenced to the residual solvent signal.

We identified peaks near 120 ppm for the NN-based copolymers in HMBC NMR (Figures S24, S28, and S32) that do not appear for OMe-ROMP (Figure S21) and designated the protons between 3.32 and 1.25 ppm to be two to three bonds away from the nitrile moiety. The aliphatic -CH signal at 2.99 ppm identified in the HSQC NMR (Figures S25, S29, and S33) was assigned to the bridgehead proton next to the nitrile through correlations observed with the backbone -CH protons at ca. 5.75-5.22 ppm in COSY (Figures S26, S30, and \$34). Since the peaks between 8.39 and 8.48 ppm correspond to the protons on the middle ring of the terminal anthracene moiety in the OMe macromonomers, we integrated the peaks relative to the backbone −CH protons at ~5.75 and 5.22 ppm to find the percentage associated with the OMe macromonomers. We determined the ratio of NN incorporated by finding the difference and dividing it by the percentage associated with OMe macromonomers. For the N-based copolymers, we identified the peaks at 2.82 and 2.46 ppm to be the bridgehead protons of cis and trans poly(N) segments by HSQC NMR (Figures S37 and S41). We followed the same procedure as described for the NN-based copolymers to determine the ratio of N to OMe macromonomers in ¹H NMR (Figures S35 and S39) to determine the ratio of N to OMe macromonomers. To identify the -C≡N functional group in NN-based copolymers, infrared spectra were collected using a Thermo Fisher FTIR6700 spectrometer in the attenuated total reflection (ATR) mode for a total of 32 scans between the 500 and 4000 cm⁻¹ range using a resolution of 4 cm⁻¹.

Molecular weight and dispersity of CN-ROMP were obtained using preparative gel permeation chromatography performed on a LabACE LC-5060 recycling preparative HPLC containing refractive index and ultraviolet detectors and equipped with a JAIGEL-2.5HR column from Japan Analytical Industry. All runs were performed in HPLC-grade chloroform at a flow rate of 10 mL min $^{-1}$ at room temperature. Molecular weight and dispersity of the copolymers were obtained using an Agilent 1260 Infinity system with a guard column (Agilent PLgel; 5 μ m; 50 mm \times 7.5 mm) and three analytical columns (Agilent PLgel; 5 μ m; 300 mm \times 7.5 mm; 10 $^{\rm S}$, 10 $^{\rm 4}$, and 10 $^{\rm 3}$ Å pore sizes). The instrument was calibrated with polystyrene standards between 1.7 and 3150 kg mol $^{-1}$. All runs were performed in HPLC-grade tetrahydrofuran at 1.0 mL min $^{-1}$ flow rate and 35 °C. Molecular weight values were calculated using ChemStation GPC data analysis software (rev. B.01.01) based on the refractive index signal.

Thermal Characterization. The thermal stability of the copolymers was evaluated under nitrogen atmosphere (Airgas, ultrahigh-purity grade) using a TGA 550 from TA Instruments. The heating ramp speed was set to 10 °C min $^{-1}$ between room temperature and 900 °C. Differential scanning calorimetry (DSC) measurements were performed on a DSC 250 from TA Instruments using a heating and cooling rate of 10 °C min $^{-1}$ from 26 to 300 °C. Glass transition temperatures were determined using the last trace of the cyclic heating cycle. Dynamic mechanical analysis (DMA) measurements were performed on a DMA Q850 from TA Instruments with the oscillation temperature ramp mode at a frequency of 1 Hz, 20 $\mu \rm m$ amplitude, and heating rate of 3 °C min $^{-1}$ between 26 and 300 °C. Film samples of 5.3 mm \times 15 mm \times 0.05 mm dimensions were prepared for testing.

Physical Characterization. The physical packing structure of the copolymers was evaluated with wide-angle X-ray scattering (WAXS), scanning electron microscopy (SEM), Brunauer–Emmett–Teller (BET) analysis, density measurements, and fractional free volume (FFV) calculations. WAXS measurements were collected on a SAXSLAB instrument equipped with a DECTRIS PILATUS 300K detector and a Rigaku 002 microfocus X-ray source. Each measurement was taken under a 0.08 mbar vacuum for 300 s in the 3–70 Å

Scheme 2. Synthesis of CN Macromonomers (4)

range. Measurements were taken from the forward direction of radiation as a function of scattering angle, 2θ . The scattering profile was normalized to a wavelength-independent scale through conversion to momentum transfer, q

$$q = 4\pi \sin \theta / \lambda \tag{1}$$

where θ is 1/2 the scattering angle and λ is the wavelength in Ångstroms. The d-spacing, d, is then calculated from the relation shown in eq 2.

$$q = 2\pi/d \tag{2}$$

SEM images were collected on a Zeiss Gemini 450 SEM at a 40K magnification. Polymer films were coated in 20 nm gold before imaging. N_2 BET isotherms were measured at 77 K and BET surface areas were determined using a Micromeritics 3Flex analyzer. All samples were degassed under high vacuum at 120 $^{\circ}\text{C}$ for 12 h prior to analysis. Bulk films were cut into circular pieces with a 5 mm diameter using a 5 mm hollow steel punch (General Tools MFG. Co., Inc.). The thickness of the films was measured using a micrometer. The film volume was calculated as the volume of a cylinder, with the thickness as the height. The weight of each circular film was measured by using a microbalance. Density was calculated by dividing the weight by the volume of each circular film.

The FFV was calculated for each polymer using eq 3

$$FFV = \frac{V - 1.3V_W}{V} \tag{3}$$

where V is the molar volume of the polymer (cm³ mol⁻¹) and $V_{\rm W}$ is the van der Waals volume of the polymer (cm³ mol⁻¹) determined using the group contribution method updated by Wu et al.²⁷

Pure-gas Sorption Analysis. Sorption isotherms for CH_4 and CO_2 were measured at 35 °C up to ~48 bar by an automated pressure decay method using a dual volume and dual transducer sorption system from Maxwell Robotics. Approximately 130–145 mg of polymer film was loaded into the sample cell and sealed with a VCR gasket. Each sample was degassed for at least 15 h at 35 °C before beginning an experiment. The system was also degassed for 4 h when switching between CH_4 and CO_2 . Equilibrium hold times for each pressure step were set to 1.5 h for CH_4 and 0.8 h for CO_2 . We report fugacity based on the second virial equation of state to correct for nonidealities.

The amount of moles sorbed into the polymer was determined for each equilibrium fugacity point using a mole balance between the initial and equilibrium conditions. ²⁹ Isotherms were then fitted using the dual-mode sorption (DMS) model

$$C = k_{\rm D}f + \frac{C'_{\rm H}bf}{1 + bf} \tag{4}$$

where C is the concentration of gas in the polymer $(cm_{STP}^3 cm_{pol}^{-3})$, f is the equilibrium fugacity (atm), $k_{\rm D}$ is Henry's constant $(cm_{STP}^3 cm_{pol}^{-3})$ atm⁻¹), $C_{\rm H}'$ is the Langmuir capacity constant $(cm_{STP}^3 cm_{pol}^{-3})$, and b is the Langmuir affinity constant (atm⁻¹). The fit was performed via nonlinear optimization using the χ^2 parameter as the objective function, and uncertainties used for the χ^2 parameter were determined from error propagation. Each gas—polymer pair was optimized independently. Error for $k_{\rm D}$, $C_{\rm H}'$, and b were determined by varying each parameter (while all other parameters are fixed) about a quadratic estimation of χ^2 with respect to the varied parameter.

The sorption coefficient can be calculated by dividing the concentration by the corresponding fugacity

$$S = \frac{C}{f} = k_{\rm D} + \frac{C'_{\rm H}b}{1 + bf} \tag{5}$$

The diffusion coefficient was back-calculated for samples evaluated in equilibrium sorption analysis using the solution—diffusion model³²

$$D = \frac{P}{S} \tag{6}$$

The sorption coefficient at infinite dilution, $S_{\text{in}\theta}$ can be determined by taking the limit of eq 5 as the fugacity approaches zero

$$\lim_{f \to 0} S = S_{\inf} = k_{\mathcal{D}} + C'_{\mathcal{H}}b \tag{7}$$

Error for sorption coefficients and diffusion coefficients calculated from equilibrium sorption analysis were determined using error propagation of the relative errors in k_D , C'_H , b, and P.

Pure-Gas Permeation Analysis. An automated constant-volume, variable-pressure permeation system from Maxwell Robotics was used to collect pure-gas permeation measurements of samples. Polymer films $50-98~\mu m$ were cut and glued to the edges of a hole in the center of a brass disk using epoxy glue (Devcon 5 min Epoxy). Once the glue dried, polymer samples were loaded and sealed into a stainless-steel permeation cell, dosed with \sim 2 bar of helium gas to remove residual gas in the system, and degassed for 8 h at 35 °C before the beginning of an experiment. The permeabilities of He, H₂, CH₄, N₂, O₂, and CO₂ were determined at \sim 1 bar. For plasticization studies, sample permeabilities were collected for consecutively increasing CO₂ pressures from 1–51 bar. Before switching to a new gas, samples were dosed with \sim 2 bar of helium and then degassed for at least 1 h.

Pure-gas permeability (P) was calculated using the following equation

Table 1. Structure and Name of Copolymers Synthesized for This Study

Structure	Comonomer	Statistical or block copolymer	Molar eq. (x:m)	Name
OMe OMe	Nitrile norbornene (NN)	Statistical	13	NN-13
Meo Meo	Nitrile norbornene (NN)	Statistical	3	NN-3
OMe OMe	Norbornene (N)	Statistical	19	N-19
MeO MeO	Norbornene (N)	Statistical	3	N-3
OMe OMe MeO	Nitrile norbornene (NN)	Block	24	NNb-24

"Molar equivalents of norbornene (N) and nitrile norbornene (NN) compared to macromonomers determined by NMR in each copolymer are included.

$$P = \frac{V_{\rm d}l}{p_2 ART} \left[\left(\frac{\mathrm{d}p}{\mathrm{d}t} \right)_{\rm SS} - \left(\frac{\mathrm{d}p}{\mathrm{d}t} \right)_{\rm leak} \right] \tag{8}$$

where $V_{\rm d}$ is the volume downstream of the film, l is the film thickness, p_2 is the upstream pressure, A is the area of film exposed to the gas, R is the ideal gas constant, T is the absolute experimental temperature, $\left(\frac{{\rm d}p}{{\rm d}t}\right)_{\rm SS}$ is the rate of pressure rise in the permeate at steady state, and $\left(\frac{{\rm d}p}{{\rm d}t}\right)_{\rm leak}$ is the leak rate. Phe ideal gas selectivity $(\alpha_{i,j})$ was taken to be the ratio of the pure-gas permeabilities of the more permeable gas, i, to that of the less permeable gas, j (i.e., $\frac{P_i}{P_j}$). The time lag, θ , was determined and diffusion coefficients were calculated using the time-lag method for each gas. The state of the series of

$$D = \frac{l^2}{6\theta} \tag{9}$$

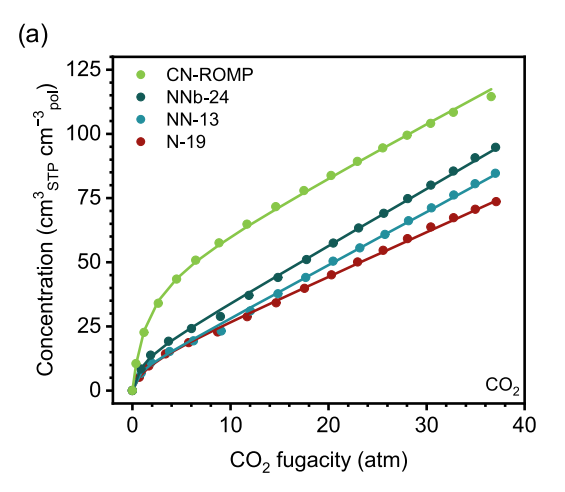
For He and $\rm H_2$, the diffusion coefficients were sometimes outside the acquisition time resolution of the permeation system (approximately 1–2 s), so the diffusion coefficients for these two gases are not reported. Sorption coefficients derived from the time lag were calculated using the sorption–diffusion model.³²

$$S = \frac{P}{D} \tag{10}$$

Error was calculated as the standard deviation of triplicate measurements.

RESULTS AND DISCUSSION

The synthesis of CN macromonomers was achieved in four steps (Scheme 2). First, 2,3-dimethylnaphthalene was brominated using Wohl-Ziegler conditions to yield 2,3-bis-(bromomethyl)naphthalene (1). The bromides were then substituted with cyanides to give 2,3-bis(cyanomethyl)naphthalene (2). Following the substitution, we performed a condensation reaction with 2,3-bis(cyanomethyl)naphthalene and 2,3-dione-5-norbornene to produce the CN-ROMP monomer (3). To synthesize the CN-based macromonomers (4), the neat Diels-Alder of the CN-ROMP monomer required a higher temperature (274 °C) than the OMe- and CF₃- analogues. 15,16 There are reports of ruthenium-based catalysts tolerating simple nitrile groups; 34-38 however, the ROMP of the CN-based macromonomers was unsuccessful with Grubbs and Hoveyda-Grubbs catalysts. This observation suggests the deactivation of the catalyst may involve more than simple coordination and perhaps include charge transfer to the electron-poor 1,4-dicyano-aryl moiety.³⁹ Schrock's catalyst has been used to make CN-containing ROMP polymers previously, 40 so we switched to Schrock's catalyst to successfully synthesize CN-ROMP (Scheme 1a). The molec-



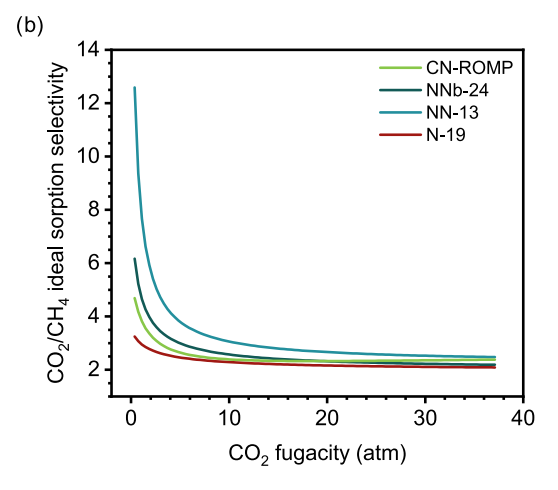


Figure 1. (a) Pure-gas CO₂ sorption isotherms with dual-mode model fits and (b) ideal CO₂/CH₄ sorption selectivity for CN-ROMP, NNb-24, NN-13, and N-19 copolymers.

ular weight of CN-ROMP was lower than that of our previously reported ROMPs 15,16 and we were unable to fabricate free-standing films for permeation characterization. In addition to this challenge, repeated polymerization attempts were inconsistent, sometimes yielding lower molecular weight (<35 kDa $M_{\rm n}$) or no polymer. Polymerizing OMe macromonomers with Schrock's catalyst resulted in oligomers with 11.8 kDa $M_{\rm n}$. Copolymerizing the CN and OMe macromonomers with Schrock's catalyst resulted in oligomers and not in the high-molecular-weight polymer needed to produce films. We suspect that the length of the larger macromonomer side chains may also hinder the polymerization. Consequently, we chose to synthesize copolymers using OMe-based oligomers with Grubbs second generation to reduce inconsistencies.

We copolymerized the OMe macromonomers with NN or N using a one-pot synthesis to produce statistical copolymers for this study (Table 1). A series of copolymers as NN-X or N-X were produced, where X is the molar ratio of NN or N to OMe macromonomer determined using HMBC, HSQC, and ¹H NMR (see the Experimental Section for more details). For instance, a copolymer containing 13:1 NN to OMe macromonomer would be labeled as NN-13. Likewise, a copolymer containing 3:1 N to OMe macromonomer would be labeled as N-3. Given the significantly higher molecular weight of the OMe macromonomer, statistical copolymers produced with 50 wt % NN or N loading yielded NN-13 and N-19, respectively. Additionally, we suspect the nitriles are coordinating with the ruthenium center,³⁹ inducing slower propagation and reducing OMe macromonomer incorporation efficiencies. Longer OMe macromonomers present in the reaction mixture may also hinder propagation. Decreasing the loading of NN to 27.5 wt % produced statistical copolymer NN-3 while a 26.3 wt % loading of N gave statistical copolymer N-3. We note that N-3 had the broadest polydispersity (D = 5.5) (Table S1) compared to all of the other copolymers, suggesting intraand interchain side reactions occurred. The NN-based block copolymer, NNb-24, made with 50 wt % NN loading was also prepared for this study. We confirmed successful formation of the block copolymer by analyzing the retention time of polymer aliquots before and after the addition of NN (Figure S2).

The characteristic $-C \equiv N$ stretch signal near 2260 cm⁻¹ was identified in IR spectroscopy (Figure S3) for all NN-based

copolymers, thereby confirming the successful incorporation of NN. OMe-ROMP does not show a measurable $T_{\rm g}$ below its degradation temperature; however, poly(N) and poly(NN) homopolymers do have accessible $T_{\rm g}$ s. Poly(NN) and poly(N) homopolymers have high thermal stability with a $T_{\rm d,5}$ temperature of 401 and 398 °C, respectively (Figure S4). The $T_{\rm g}$ s are observed at 136 and 45 °C for poly(NN) and poly(N), respectively (Figure S5), which are close to values reported in the literature. S5, which are close to values reported in the literature. All of the copolymers show excellent thermal stability with $T_{\rm d,5}$ temperatures between 336 and 345 °C (Figure S4). The statistical copolymers NN-13 and N-19 exhibit $T_{\rm g}$ s at ~224 and 78 °C, respectively, as revealed by DSC and DMA analysis (Figures S5 and S6). The $T_{\rm g}$ of block copolymer NNb-24 was found to be 176 °C (Figure S5).

The pure-gas CO₂ sorption and CO₂/CH₄ sorption selectivity measured at 35 °C of CN-ROMP, block copolymer NNb-24, and statistical copolymers N-19 and NN-13 are presented in Figure 1. We observed the highest CO₂ sorption in CN-ROMP and greater CO2 sorption with increasing nitrile content in the copolymers (Figure 1a). Moreover, when compared to OMe-ROMP homopolymers, CN-ROMP had a higher overall sorption, demonstrating the benefits of CN incorporation and high BET surface area of this material (Figure S1a and Table S1). The relative order of ideal CO_2 / CH₄ sorption selectivity (NN-13 > NNb-24 > N-19) shown in Figure 1b confirms that nitriles boost the selectivity for CO₂. We noted a decrease in ideal CO₂/CH₄ sorption selectivity at high CO₂ pressure for all polymers tested that is similar to that observed for PIM-1, PIM-NH2, PIM-COOH, and PIMdeBOC. In the case for PIM-1 and its analogues, mixed-gas testing revealed a minimal decrease in CO₂/CH₄ sorption selectivity at high CO₂ pressure resulting from dual-mode sorption effects.²⁵ Our previous studies identified pore size distributions for poly(OMe 4-mer) and polydisperse OMe-ROMP averaging near ~10 Å.17 When collecting WAXS data of the copolymers, we observed an additional diffuse scattering peak at ~10.3 Å for NNb-24 that is not present for NN-13 or the poly(NN) homopolymer (Figure S7a). Thus, we attributed the larger *d*-spacing associated with voids to inefficient polymer chain packing from the rigid macromonomer block.⁴² The SEM images of N-19, NN-13, and NNb-24 are provided in Figure S8. The films made from the statistical copolymers exhibit a smooth, amorphous texture at 40K magnification, while patterns were observed on the block copolymer film at

Table 2. CH₄ and CO₂ Sorption at Infinite Dilution (S_{inf}) for N-19, NN-13, NNb-24, and CN-ROMP^a

gas	N-19	NN-13	NNb-24	CN-ROMP	poly(OMe 5-mer) ¹⁸	PIM-1 ²⁵
CH ₄	3.17 ± 0.1	0.917 ± 0.009	2.40 ± 0.5	6.43 ± 0.07	5.70	9.64
CO_2	11.2 ± 0.3	19.1 ± 1.7	19.1 ± 1.1	35.19 ± 0.04	20.0	48.0

"Data for poly(OMe 5-mer)18 and PIM-125 is included for comparison. Sinf is given in units of cm3STP cm-3pol atm-1.

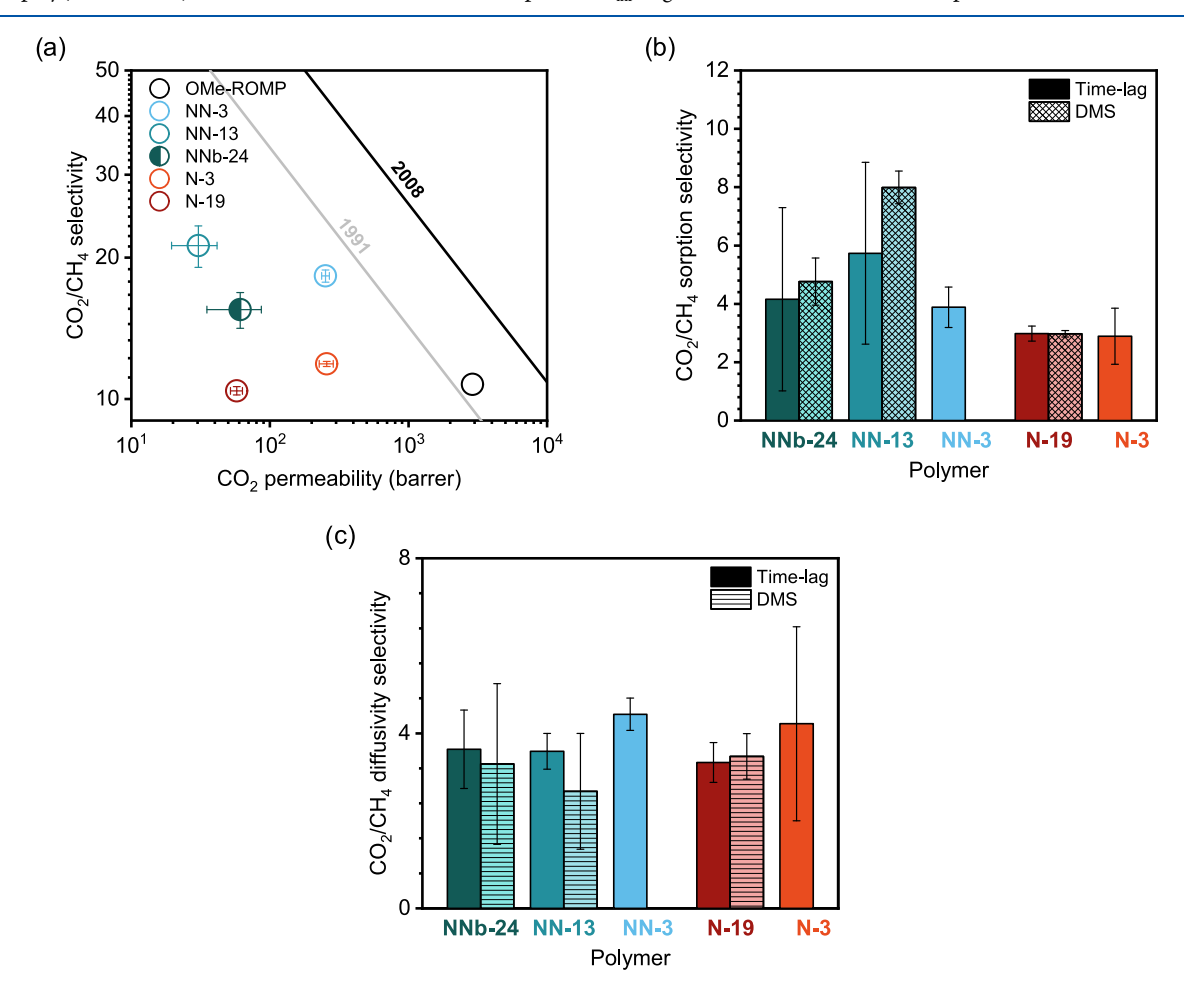
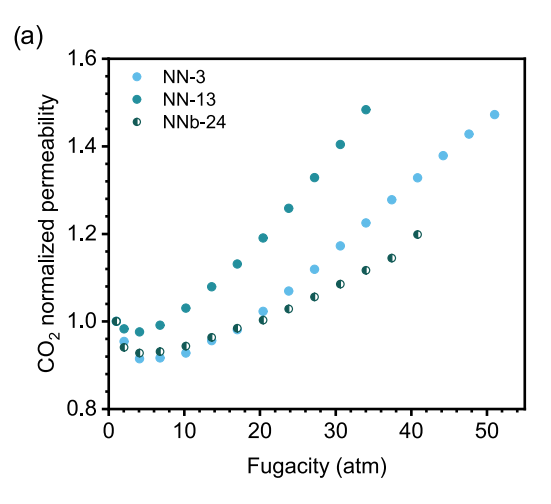


Figure 2. Pure-gas (a) permeation of CO_2/CH_4 for NN- and N-based copolymers compared to OMe-ROMP¹⁷ measured at 35 °C and 1 atm, (b) CO_2/CH_4 sorption selectivity calculated from permselectivity divided by time-lag diffusivity selectivity measurements for each copolymer, and (c) CO_2/CH_4 diffusivity selectivity calculated from time-lag for each copolymer. Panels (b) and (c) also contain selectivity derived from static equilibrium sorption measurements for NNb-24, NN-13, and N-19. These results are reported as DMS results in the figure.

the same magnification. We suspect the statistical copolymer architecture enables NN comonomers to occupy free volume generated by the rigid macromonomers, resulting in the smooth texture in SEM and the absence of larger *d*-spacing values. When the macromonomers are in a block sequence, this appears to partially preserve the poly(OMe) homopolymer morphology.

We calculated dual-mode sorption (DMS) parameters for CN-ROMP, NNb-24, NN-13, and N-19 to investigate the sorption behavior of CO_2 and CH_4 (Table S2) and to help with extracting values of sorption at infinite dilution, $S_{\rm inf}$. The Langmuir affinity constant, b, is an equilibrium constant that describes the likelihood of a specific penetrant to sorb within the Langmuir mode. Sinf is a material property that describes the partitioning of the first penetrant from the gas phase into the polymer matrix. DMS fitting was successful for all polymers tested except for the CH_4 isotherm of NN-13 due to its linearity. Thus, we fitted the CH_4 isotherm data for NN-13 to Henry's law as an approximation. We note that CN-ROMP

shows higher b and S_{inf} parameters for CO₂ than poly(OMe 5mer), 18 confirming nitriles enhance affinity for CO2 relative to methoxy groups. Parameters b and S_{inf} from the CO_2 sorption isotherm are larger for copolymer NNb-24 and NN-13 than N-19, indicating the NN-based copolymers have greater affinity for CO₂ than N-19 (Tables 2 and S2). Despite greater nitrile content, block copolymer NNb-24 exhibits the same S_{inf} and lower b for CO₂ than that for statistical copolymer NN-13. The decrease in b appears to be compensated for by a larger Langmuir capacity constant, C'_{H} , which could be an artifact of least-squares fitting with these coupled parameters. The same trend in C'_H values (NN-13 < N-19 < NNb-24) is observed in BET surface areas (Table S1). Furthermore, the physical meaning of C'_H is not well defined in these phenomenological models, so we decline from drawing robust conclusions with this comparison. ^{6,45} Compared to PIM-1, S_{inf} is ~27% lower in CN-ROMP. When studying sorption in monodisperse OMe-ROMP, we noted improvements in S_{inf} as side-chain length



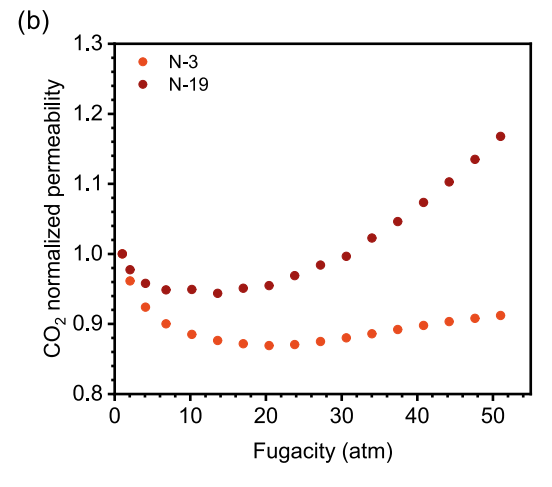


Figure 3. Normalized CO₂ permeabilities for high pressure sweeps of (a) NN- and (b) N-based copolymers.

increased, 18 suggesting monodisperse CN-ROMP with longer side chains could improve S_{inf}

The expected higher CO₂/CH₄ selectivity for the NN-based copolymers is observed in pure-gas permeation tests (Figure 2a). We found the NN-3 statistical copolymer exhibits a 1.3and 1.7-fold increase in CO₂/CH₄ selectivity compared to N-3 and OMe-ROMP, 17 respectively. Nevertheless, increasing nitrile content from NN-3 to NN-13 provides minimal enhancement to CO₂/CH₄ selectivity and reduces the gas throughput by 1 order of magnitude. In contrast, the block copolymer NNb-24 displayed a 2-fold increase in permeability compared with the statistical copolymer NN-13 and an ~27% decrease in CO₂/CH₄ selectivity. We attribute this decrease in selectivity to a greater diffusivity through excess free volume of the OMe block identified via WAXS and SEM (Figures S7a and S8c) within the rigid macromonomer. To better understand the gas transport behavior, we tabulated diffusivity and sorption coefficients calculated from the time-lag method and compared trends in gas transport among all copolymers tested (Table S3). We observed an ~2-fold increase in CO₂/ CH₄ sorption selectivity for NN-13 relative to N-19 when using coefficients obtained from the time-lag calculations (Figure 2b and Table S3). We noted a similar increase using data from equilibrium sorption measurements (Table S3), and hence, these results cannot be attributed to artifacts from only considering transport diffusivities. Furthermore, the time-lag method is known to have large uncertainties in lab-to-lab studies, 46 so the equilibrium measurements are helpful for us to report more statistically robust conclusions. Figure 2b and Table S4 further reveal that NNb-24 displays similar CO₂/CH₄ sorption selectivity to that of NN-3 despite its higher nitrile content. In Figure 2c and Table S4, the CO₂/CH₄ diffusivity selectivity in NN-3 and N-3 copolymers is found to be greater than the rest of the copolymers and is close to the CO₂/CH₄ diffusivity selectivity reported for poly(OMe 4-mer). Copolymers with larger amounts of N and NN show similar CO₂/CH₄ diffusivity selectivity, so differences in gas transport between the copolymers arise from changes in CO₂/CH₄ sorption selectivity.

We expected that changes in density of the ladder polymer side chains would impact the exceptional plasticization resistance exhibited by OMe-ROMP, 16,17 so we investigated the stability against CO₂ plasticization of each copolymer with pressure-increase experiments (Figure 3). The plasticization pressure remained at \sim 4 bar of CO₂ pressure for all NN-based

copolymers tested. However, decreasing nitrile content or using a blocky morphology was observed to lower the rate of increase in the CO₂ permeability, thereby elevating stability against CO₂ plasticization (Figure 3a). The N-based copolymers showed higher plasticization pressures (~20 bar) at lower levels of incorporation of N (Figure 3b). This finding may relate to the lower CO₂ sorption in the N polymers, which would result in reduced $T_{\rm g}$ suppression and hence a resistance to enhanced corporative chain motion, which is the origin of plasticization. 47 This tunability of the CO₂ plasticization pressure is similar to what was observed with increasing the length of the rigid, pore-generating side chains in OMe-ROMP. Our results suggest a higher density of the rigid ladder oligomer side-chain macromonomers promotes greater stability against CO2 plasticization. Additionally, the concentration of CO2 at the plasticization pressures determined for NN-13 and NNb-24 (15.2 and 19.5 cm_{STP} cm_{pol}, respectively) were outside of the critical CO₂ concentration range determined by Bos et al. in 1999.⁴⁸ Mixed-gas permeation experiments enrich our understanding of the competitive effects arising from the presence of nitriles and will be the focus of future studies of these statistical and block copolymer architectures.

CONCLUSIONS

Pure-gas sorption of CN-ROMP and transport of five copolymers based on OMe-ROMP were evaluated to investigate the role of free volume promoting ladder side chains and nitrile incorporation in CO₂/CH₄ selectivity and CO₂ plasticization. Equilibrium sorption analysis and permeation experiments confirmed our hypothesis that nitriles enhance the CO₂ sorption affinity and the CO₂/CH₄ permselectivity. Our findings also revealed that the density and connectivity of the rigid, pore-generating side chains influenced transport properties. Decreasing density of the rigid side chains in NN-13 resulted in an ~40% increase in CO₂/ CH₄ sorption selectivity compared to the block copolymer NNb-24. Moreover, we also observed a 50% increase in CO₂ and CH₄ diffusivity for NNb-24 compared to that for NN-13, suggesting a benefit to using a block copolymer approach to enhance diffusivity even with a lower concentration of poregenerating ladder side chains. This finding was supported through WAXS and SEM analysis, which demonstrated that blocks of free-volume-generating macromonomers could

preserve the high free-volume features found in poly(ladder) homopolymers. Greater stability against CO_2 plasticization was also attributed to a higher density of the rigid macromonomers. This study introduces a CO_2 -philic functional group through copolymerization that improves CO_2 selectivity and highlights the structure—property relationships between the density of pore-generating side chains, backbone functionalization, gas transport, and plasticization stability in an emerging class of PIM materials.

ASSOCIATED CONTENT

Solution Supporting Information

The Supporting Information is available free of charge at https://pubs.acs.org/doi/10.1021/acs.macromol.3c02348.

¹H, ¹³C, HMBC, HSQC, and COSY NMR, FT-IR, TGA, DSC, DMA, BET, WAXS spectra, SEM images, SEC and density data, CH₄ equilibrium sorption isotherms, tabulated dual-mode sorption (DMS) parameters calculated using different fit constraints, permeation data, diffusion and sorption coefficients calculated using the time-lag method, dual-mode sorption parameters, and sorption—diffusion model, and CO₂ high pressure sweeps (PDF)

AUTHOR INFORMATION

Corresponding Authors

Zachary P. Smith – Department of Chemical Engineering, Massachusetts Institute of Technology, Cambridge, Massachusetts 02139, United States; orcid.org/0000-0002-9630-5890; Email: zpsmith@mit.edu

Timothy M. Swager — Department of Chemistry, Massachusetts Institute of Technology, Cambridge, Massachusetts 02139, United States; oocid.org/0000-0002-3577-0510; Email: tswager@mit.edu

Authors

Kayla R. Storme – Department of Chemistry, Massachusetts Institute of Technology, Cambridge, Massachusetts 02139, United States

Sharon Lin — Department of Chemical Engineering, Massachusetts Institute of Technology, Cambridge, Massachusetts 02139, United States; Oorcid.org/0000-0001-7566-482X

You-Chi Mason Wu – Department of Chemistry, Massachusetts Institute of Technology, Cambridge, Massachusetts 02139, United States

Sherrie X. Qian – Department of Materials Science and Engineering, Massachusetts Institute of Technology, Cambridge, Massachusetts 02139, United States

Complete contact information is available at: https://pubs.acs.org/10.1021/acs.macromol.3c02348

Notes

The authors declare no competing financial interest.

ACKNOWLEDGMENTS

The synthetic design of materials to incorporate pore architecture was supported by the U.S. Department of Energy, Office of Science, Office of Basic Energy Sciences, Separation Science program through award number DE-SC0019087. The authors also gratefully acknowledge the Office of Naval Research under award number N00014-21-1-2666 for

developing strategies related to site-specific CO_2 binding. K.R.S. acknowledges support from the National Science Foundation Graduate Research Fellowship under grant number 1745302. T.M.S. is grateful for funding from the National Science Foundation (DMR-2207299). This work made use of the MRSEC Shared Experimental Facilities at MIT, supported by the National Science Foundation under award number DMR-1419807. This work was also carried out in part through the use of MIT.nano's facilities.

REFERENCES

- (1) Sholl, D. S.; Lively, R. P. Seven Chemical Separations to Change the World. *Nature* **2016**, *532*, 435–437.
- (2) DOE-EPSA. Energy CO₂ Emiss. Impacts Clean Energy Technol. Innov. Policy Energy CO₂ Emiss. Impacts Clean Energy Technol. Innov. Policy **2017**, 43.
- (3) Baker, R. W. Future Directions of Membrane Gas Separation Technology. *Ind. Eng. Chem. Res.* **2002**, *41* (6), 1393–1411.
- (4) Galizia, M.; Chi, W. S.; Smith, Z. P.; Merkel, T. C.; Baker, R. W.; Freeman, B. D. 50th Anniversary Perspective: Polymers and Mixed Matrix Membranes for Gas and Vapor Separation: A Review and Prospective Opportunities. *Macromolecules* **2017**, *50* (20), 7809–7843.
- (5) Koros, W. J.; Zhang, C. Materials for Next-Generation Molecularly Selective Synthetic Membranes. *Nat. Mater.* **2017**, *16* (3), 289–297.
- (6) Minelli, M.; Sarti, G. C. 10th Anniversary: Gas and Vapor Sorption in Glassy Polymeric Membranes-Critical Review of Different Physical and Mathematical Models. *Ind. Eng. Chem. Res.* **2020**, *59* (1), 341–365.
- (7) Long, T. M.; Swager, T. M. Molecular Design of Free Volume as a Route to Low-κ Dielectric Materials. *J. Am. Chem. Soc.* **2003**, *125* (46), 14113–14119.
- (8) Li, P.; Chung, T. S.; Paul, D. R. Gas Sorption and Permeation in PIM-1. *J. Membr. Sci.* **2013**, 432, 50–57.
- (9) Comesaña-Gándara, B.; Chen, J.; Bezzu, C. G.; Carta, M.; Rose, I.; Ferrari, M.-C.; Esposito, E.; Fuoco, A.; Jansen, J. C.; McKeown, N. B. Redefining the Robeson Upper Bounds for $\rm CO_2/CH_4$ and $\rm CO_2/N_2$ Separations Using a Series of Ultrapermeable Benzotriptycene-Based Polymers of Intrinsic Microporosity. *Energy Environ. Sci.* **2019**, *12* (9), 2733–2740.
- (10) Park, H. B.; Jung, C. H.; Lee, Y. M.; Hill, A. J.; Pas, S. J.; Mudie, S. T.; Van Wagner, E.; Freeman, B. D.; Cookson, D. J. Polymers with Cavities Tuned for Fast Selective Transport of Small Molecules and Ions. *Science* **2007**, *318* (5848), 254–258.
- (11) Lai, H. W. H.; Benedetti, F. M.; Ahn, J. M.; Robinson, A. M.; Wang, Y.; Pinnau, I.; Smith, Z. P.; Xia, Y. Hydrocarbon Ladder Polymers with Ultrahigh Permselectivity for Membrane Gas Separations. *Science* **2022**, 375 (6587), 1390–1392.
- (12) Lai, H. W. H.; Benedetti, F. M.; Jin, Z.; Teo, Y. C.; Wu, A. X.; Angelis, M. G. De.; Smith, Z. P.; Xia, Y. Tuning the Molecular Weights, Chain Packing, and Gas-Transport Properties of CANAL Ladder Polymers by Short Alkyl Substitutions. *Macromolecules* **2019**, 52 (16), 6294–6302.
- (13) Zhang, C.; Fu, L.; Tian, Z.; Cao, B.; Li, P. Post-Crosslinking of Triptycene-Based Tröger's Base Polymers with Enhanced Natural Gas Separation Performance. *J. Membr. Sci.* **2018**, *556*, 277–284.
- (14) Swaidan, R.; Ghanem, B.; Litwiller, E.; Pinnau, I. Physical Aging, Plasticization and Their Effects on Gas Permeation in "Rigid" Polymers of Intrinsic Microporosity. *Macromolecules* **2015**, 48 (18), 6553–6561.
- (15) Zhao, Y.; He, Y.; Swager, T. M. Porous Organic Polymers via Ring Opening Metathesis Polymerization. *ACS Macro Lett.* **2018**, 7 (3), 300–304.
- (16) He, Y.; Benedetti, F. M.; Lin, S.; Liu, C.; Zhao, Y.; Ye, H. Z.; Van Voorhis, T.; De Angelis, M. G.; Swager, T. M.; Smith, Z. P. Polymers with Side Chain Porosity for Ultrapermeable and

- Plasticization Resistant Materials for Gas Separations. *Adv. Mater.* **2019**, *31* (21), 1–8.
- (17) Benedetti, F. M.; Wu, Y.-C. M.; Lin, S.; He, Y.; Flear, E.; Storme, K. R.; Liu, C.; Zhao, Y.; Swager, T. M.; Smith, Z. P. Side-Chain Length and Dispersity in ROMP Polymers with Pore-Generating Side Chains for Gas Separations. *JACS Au* **2022**, 2 (7), 1610–1615.
- (18) Lin, S.; Storme, K. R.; Wu, Y.-C. M.; Benedetti, F. M.; Swager, T. M.; Smith, Z. P. Role of Side-Chain Length on Gas Transport of CO₂/CH₄ Mixtures in Polymers with Side-Chain Porosity. *J. Membr. Sci.* **2023**, 668, No. 121194.
- (19) Swaidan, R.; Ghanem, B. S.; Litwiller, E.; Pinnau, I. Pure- and Mixed-Gas CO_2/CH_4 Separation Properties of PIM-1 and an Amidoxime-Functionalized PIM-1. *J. Membr. Sci.* **2014**, 457, 95–102.
- (20) Mason, C. R.; Maynard-Atem, L.; Al-Harbi, N. M.; Budd, P. M.; Bernardo, P.; Bazzarelli, F.; Clarizia, G.; Jansen, J. C. Polymer of Intrinsic Microporosity Incorporating Thioamide Functionality: Preparation and Gas Transport Properties. *Macromolecules* **2011**, 44 (16), 6471–6479.
- (21) Mizrahi Rodriguez, K.; Wu, A. X.; Qian, Q.; Han, G.; Lin, S.; Benedetti, F. M.; Lee, H.; Chi, W. S.; Doherty, C. M.; Smith, Z. P. Facile and Time-Efficient Carboxylic Acid Functionalization of PIM-1: Effect on Molecular Packing and Gas Separation Performance. *Macromolecules* **2020**, *53* (15), 6220–6234.
- (22) Jeon, J. W.; Kim, D. G.; Sohn, E. H.; Yoo, Y.; Kim, Y. S.; Kim, B. G.; Lee, J. C. Highly Carboxylate-Functionalized Polymers of Intrinsic Microporosity for CO₂-Selective Polymer Membranes. *Macromolecules* **2017**, *50* (20), 8019–8027.
- (23) Weng, X.; Baez, J. E.; Khiterer, M.; Hoe, M. Y.; Bao, Z.; Shea, K. J. Chiral Polymers of Intrinsic Microporosity: Selective Membrane Permeation of Enantiomers. *Angew. Chem., Int. Ed.* **2015**, *54* (38), 11214–11218.
- (24) Mizrahi Rodriguez, K.; Lin, S.; Wu, A. X.; Han, G.; Teesdale, J. J.; Doherty, C. M.; Smith, Z. P. Leveraging Free Volume Manipulation to Improve the Membrane Separation Performance of Amine-Functionalized PIM-1. *Angew. Chem., Int. Ed.* **2021**, *60* (12), 6593–6599.
- (25) Mizrahi Rodriguez, K.; Benedetti, F. M.; Roy, N.; Wu, A. X.; Smith, Z. P. Sorption-Enhanced Mixed-Gas Transport in Amine Functionalized Polymers of Intrinsic Microporosity (PIMs). *J. Mater. Chem. A* **2021**, 9 (41), 23631–23642.
- (26) Kawakami, Y.; Toda, H.; Higashino, M.; Yamashita, Y. Polynorbornenes with Oligodimethylsiloxanyl Substituents for Selectively Oxygen Permeable Membrane Material. *Polym. J.* **1988**, 20 (4), 285–292.
- (27) Wu, A. X.; Lin, S.; Mizrahi Rodriguez, K.; Benedetti, F. M.; Joo, T.; Grosz, A. F.; Storme, K. R.; Roy, N.; Syar, D.; Smith, Z. P. Revisiting Group Contribution Theory for Estimating Fractional Free Volume of Microporous Polymer Membranes. *J. Membr. Sci.* **2021**, 636, No. 119526.
- (28) Dymond, J. D.; Marsh, K. N.; Wilhoit, R. C.; Wong, K. C. The Virial Coefficients of Pure Gases; Springer: Berlin, 2002; Vol. 21.
- (29) Lin, H.; Freeman, B. D. Permeation and Diffusion. In *Springer Handbook of Materials Measurement Methods*; Saito, T.; Czichos, H.; Smith, I. E., Eds.; Springer: Germany, 2006; pp 371–387.
- (30) Stevens, K. A.; Smith, Z. P.; Gleason, K. L.; Galizia, M.; Paul, D. R.; Freeman, B. D. Influence of Temperature on Gas Solubility in Thermally Rearranged (TR) Polymers. *J. Membr. Sci.* **2017**, 533, 75–83.
- (31) Wu, A. X.; Drayton, J. A.; Rodriguez, K. M.; Benedetti, F. M.; Qian, Q.; Lin, S.; Smith, Z. P. Elucidating the Role of Fluorine Content on Gas Sorption Properties of Fluorinated Polyimides. *Macromolecules* **2021**, *54* (1), 22–34.
- (32) Wijmans, J. G.; Baker, R. W. The Solution-Diffusion Model: A Review. J. Membr. Sci. 1995, 107, 1–21.
- (33) Frisch, H. L. The Time Lag in Diffusion. *J. Phys. Chem. A* **1957**, *61* (1), 93–95.
- (34) Belfield, K. D.; Li, Z. Norbornene-Functionalized Diblock Copolymers via Ring-Opening Metathesis Polymerization for

- Magnetic Nanoparticle Stabilization. Chem. Mater. 2006, 18 (25), 5929-5936.
- (35) Nishihara, Y.; Inoue, Y.; Saito, A. T.; Nakayama, Y.; Shiono, T.; Takagi, K. Living Ring-Opening Metathesis Polymerization of Exo-Norbornenes Bearing Both Cyano and Ester Functionalities by a Well-Defined Ruthenium Catalyst. *Polym. J.* **2007**, *39* (4), 318–329. (36) Slugovc, C.; Demel, S.; Stelzer, F. Ring Opening Metathesis
- (36) Slugovc, C.; Demel, S.; Stelzer, F. Ring Opening Metathesis Polymerisation in Donor Solvents. *Chem. Commun.* **2002**, No. 21, 2572–2573.
- (37) Demel, S.; Riegler, S.; Wewerka, K.; Schoefberger, W.; Slugovc, C.; Stelzer, F. Ruthenium-Initiated ROMP of Nitrile Monomers. *Inorg. Chim. Acta* **2003**, 345, 363–366.
- (38) Yang, D.; Huang, W.; Yu, J.; Jiang, J.; Zhang, L.; Xie, M. A Novel Shape Memory Polynorbornene Functionalized with Poly(ε -Caprolactone) Side Chain and Cyano Group through Ring-Opening Metathesis Polymerization. *Polymer* **2010**, *51* (22), 5100–5106.
- (39) Martinez, H.; Ren, N.; Matta, M. E.; Hillmyer, M. A. Ring-Opening Metathesis Polymerization of 8-Membered Cyclic Olefins. *Polym. Chem.* **2014**, *5* (11), 3507–3532.
- (40) Winkler, B.; Rehab, A.; Ungerank, M.; Stelzer, F. A Novel Side-Chain Liquid Crystal Polymer of 5-Substituted Cis-cyclooctene via Ring-Opening Metathesis Polymerization. *Macromol. Chem. Phys.* 1997, 198 (5), 1417–1425.
- (41) Hatjopoulos, J. D.; Register, R. A. Synthesis and Properties of Well-Defined Elastomeric Poly(alkylnorbornene)s and Their Hydrogenated Derivatives. *Macromolecules* **2005**, 38 (24), 10320–10322.
- (42) McDermott, A. G.; Larsen, G. S.; Budd, P. M.; Colina, C. M.; Runt, J. Structural Characterization of a Polymer of Intrinsic Microporosity: X-Ray Scattering with Interpretation Enhanced by Molecular Dynamics Simulations. *Macromolecules* **2011**, *44* (1), 14–16.
- (43) Koros, W. J. Model for Sorption of Mixed Gases in Glassy Polymers. J. Polym. Sci., Polym. Phys. Ed. 1980, 18 (5), 981–992.
- (44) Merkel, T. C.; Bondar, V.; Nagai, K.; Freeman, B. D.; Yampolskii, Y. P. Gas Sorption, Diffusion, and Permeation in Poly(2,2-bis(trifluoromethyl)-4,5-difluoro-1,3-dioxole-co-tetrafluoroethylene). *Macromolecules* 1999, 32 (25), 8427–8440.
- (45) Ricci, E.; Minelli, M.; De Angelis, M. G. Modelling Sorption and Transport of Gases in Polymeric Membranes across Different Scales: A Review. *Membranes* **2022**, *12* (9), 857.
- (46) Mizrahi Rodriguez, K.; Wu, W. N.; Alebrahim, T.; Cao, Y.; Freeman, B. D.; Harrigan, D.; Jhalaria, M.; Kratochvil, A.; Kumar, S.; Lee, W. H.; Lee, Y. M.; Lin, H.; Richardson, J. M.; Song, Q.; Sundell, B.; Thür, R.; Vankelecom, I.; Wang, A.; Wang, L.; Wiscount, C.; Smith, Z. P. Multi-Lab Study on the Pure-Gas Permeation of Commercial Polysulfone (PSf) Membranes: Measurement Standards and Best Practices. *J. Membr. Sci.* 2022, 659, No. 120746.
- (47) Mizrahi Rodriguez, K.; Lin, S.; Wu, A. X.; Storme, K. R.; Joo, T.; Grosz, A. F.; Roy, N.; Syar, D.; Benedetti, F. M.; Smith, Z. P. Penetrant-Induced Plasticization in Microporous Polymer Membranes. *Chem. Soc. Rev.* **2024**, DOI: 10.1039/D3CS00235G.
- (48) Bos, A.; Pünt, I. G. M.; Wessling, M.; Strathmann, H. CO2-Induced Plasticization Phenomena in Glassy Polymers. *J. Membr. Sci.* **1999**, *155* (1), *67*–78.